Revista Mexicana de Astronomía y Astrofísica, **59**, 155–169 (2023)

https://doi.org/10.22201/ia.01851101p.2023.59.02.01

ASTROPHYSICAL STUDIES OF 9 UNSTUDIED OPEN STAR CLUSTERS USING *GAIA DR3*

W. A. Badawy[1], A. L. Tadross[1], Y. H. M. Hendy[1], M. N. Ismail[2], and A. Mouner[2]

Received November 21 2022; accepted March 8 2023

ABSTRACT

Using the Gaia DR3 data sets, this work gives an analysis of nine open clusters: Dolidze 25, Kronberger 13, Kronberger 18, Majaess 99, NGC 7795, Ruprecht 139, Teutsch 55, S1, and FSR 0596, which are close to the Galactic plane of the Milky Way. The number of probable cluster members is found to be 81, 77, 120, 155, 108, 110, 160, and 116 respectively. Radii are determined as 5.40, 5.25, 4.80, 4.20, 4.28, 3.70, 4.30, 4.30, and 3.53 arcmin, respectively. With solar metallicity isochrones log ages of 7.70, 9.00, 8.35, 7.50, 9.00, 8.00, 7.50, 8.50, and 9.5 yr are determined for these clusters. The best fitting of the isochrone produced distances of 2.6, 1.27, 1.16, 1.16, 3.10, 1.64, 2.50, 2.44, and 0.98 kpc that are similar to the distances calculated from inverting median parallaxes. The mass function slopes are in agreement with the Salpeter value. The results of the total masses are found to be 116.07, 79.33, 141.24, 147.34, 145.76, 491.01, 155, 212.46, and 82.79 $M_{\odot}$.

RESUMEN

En este trabajo estudiamos, con datos del GAIA DR3, nueve cúmulos abiertos: Dolidze 25, Kronberger 13, Kronberger 18, Majaess 99, NGC 7795, Ruprecht 139, Teutsch 55, S1, y FSR 0596, todos ellos cercanos al plano galáctico. Encontramos que el número de miembros probables es de 81, 77, 120, 155, 108, 110, 160, y 116, respectivamente. Los radios que determinamos son: 5.40, 5.25, 4.80, 4.20, 4.28, 3.70, 4.30, 4.30, y 3.53 arcmin, respectivamente. Si suponemos isocronas con metalicidades solares los logaritmos de las edades en años son: 7.70, 9.00, 8.35, 7.50, 9.00, 8.00, 7.50, 8.50, y 9.5. El mejor ajuste de las isocronas produjo distancias de 2.6, 1.27, 1.16, 1.16, 3.10, 1.64, 2.50, 2.44, y 0.98 kpc, similares a las obtenidas a partir de las paralajes medias. Las pendientes de las funciones de masa concuerdan con el valor de Salpeter. Encontramos valores para las masas totales de 116.07, 79.33, 141.24, 147.34, 145.76, 491.01, 155, 212.46, y 82.79 $M_{\odot}$, respectivamente.

Key Words: Hertzsprung-Russell and colour-magnitude diagrams — methods: data analysis — open clusters and associations: general — stars: luminosity function, mass function

1. INTRODUCTION

To better understand the structure and evolution of the Milky Way, open clusters (OCs) are helpful probes. OCs can be used to examine the history of star evolution because they are created by the collapse and fragmentation of massive molecular clouds (Bate et al. 2003; Harris and Pudritz 1994). For more than 1.3 billion sources, the third Gaia data release (Gaia DR3) offers precise five-parameter astrometric data (positions, proper motions, and parallaxes). Gaia DR3 demonstrates how well these data can be utilized to identify cluster members, particularly in high-density areas, and it is quite successful. Over the years, OCs have been the focus of numerous studies. They are crucial and frequently utilized to understand different aspects of the Galactic disc, such as the Milky Way's spiral arms (Bonatto et al. 2006).

2. DATA ANALYSIS AND PROCEDURE

In our previous research (Badawy et al. 2022), we studied the vector point diagrams of a large sample

[1]National Research Institute of Astronomy and Geophysics, Cairo, Egypt.
[2]Faculty of Science, Al-Azhar University, Cairo, Egypt.

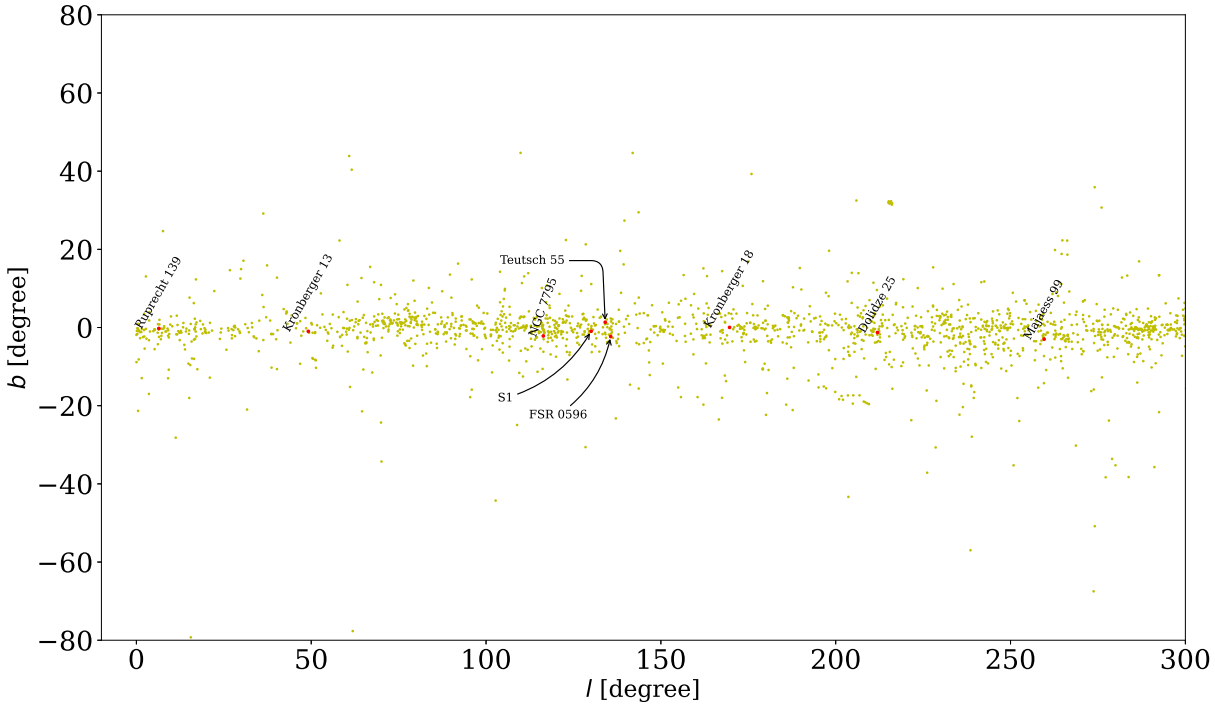

Fig. 1. The locations of the studied clusters (red dots). The yellow dots represent all the clusters obtained from Dias' catalog (Dias et al. 2014). The color figure can be viewed online.

of open stellar clusters selected from the Dais Catalog using the astrometric data of Gaia DR2. Here, we selected 9 objects that lie very close to the galactic plane and have not been studied astrometrically before using Gaia DR3 (Gaia Collaboration et al. 2022). There are full astrometric solution of positions on the sky (α, δ), parallax (ω), and proper motions (μ_α, μ_δ) for around 1.46 billion sources, with a limiting magnitude of about $G \approx 21$. We used the library Astroquery to obtain Gaia data. Astroquery is an Astropy-affiliated package that contains a collection of tools to access online astronomical data.The standard dataset of these clusters was downloaded from *Astroquery.gaia* package[3]. Using the library python package `(astroquery.simbad)`[4] we can get the central coordinates of our clusters. The source data were downloaded from the Gaia DR3 database service with radii of 0.2 degrees This package allows access to the European Space Agency Gaia Archive[5]. From the Dias catalog (Dias et al. 2014), the open clusters under study were selected and distributed according latitude and longitude, as shown in Figure (1), where the red dots represent the open clusters that are currently being studied, while the yellow dots represent all the open clusters in the catalog.

In order to select the membership, we follow the following steps. The vector point diagram (VPD) of proper motions is very useful in identifying field stars from the member stars of a cluster (Yadav et al. 2013; Straižys et al. 2019; Tadross and Hendy 2021, 2022). The vector point diagrams for all clusters are shown in Figure 2. The densest area of the cluster was placed in a sub-circle with a radius of 0.2 deg. Figure 3 shows those member stars that move at the same speed and direction in the sky (co-moving stars). The position uncertainties are $0.01 - 0.02$ mas for $G < 15$, 0.05 mas at $G = 17$, 0.4 mas at $G = 20$, and 1.0 mas at $G = 21$ mag. Due to the high accuracy of Gaia DR3, we use the sources that have $G \leq 20.5$ mag. The proper motion uncertainties are $0.02 - 0.03$ mas/yr for $G < 15$, 0.07 mas/yr at $G = 17$, 0.5 mas/yr at $G = 20$, and 1.4 mas/yr at $G = 21$ mag. The condition of 3σ for proper motions was applied to the member stars. The 3σ error in parallax was also calculated for the mean and median of the cluster. If a star of 3σ parallax error is found within the cluster mean parallax and lies inside the cluster's region, it is considered to be a member star. If we take 2σ parallax errors in-

[3] `https://astroquery.readthedocs.io/en/latest/gaia/gaia.html`
[4] `https://astroquery.readthedocs.io/en/latest/simbad/simbad.html`
[5] `http://gea.esac.esa.int/archive/`

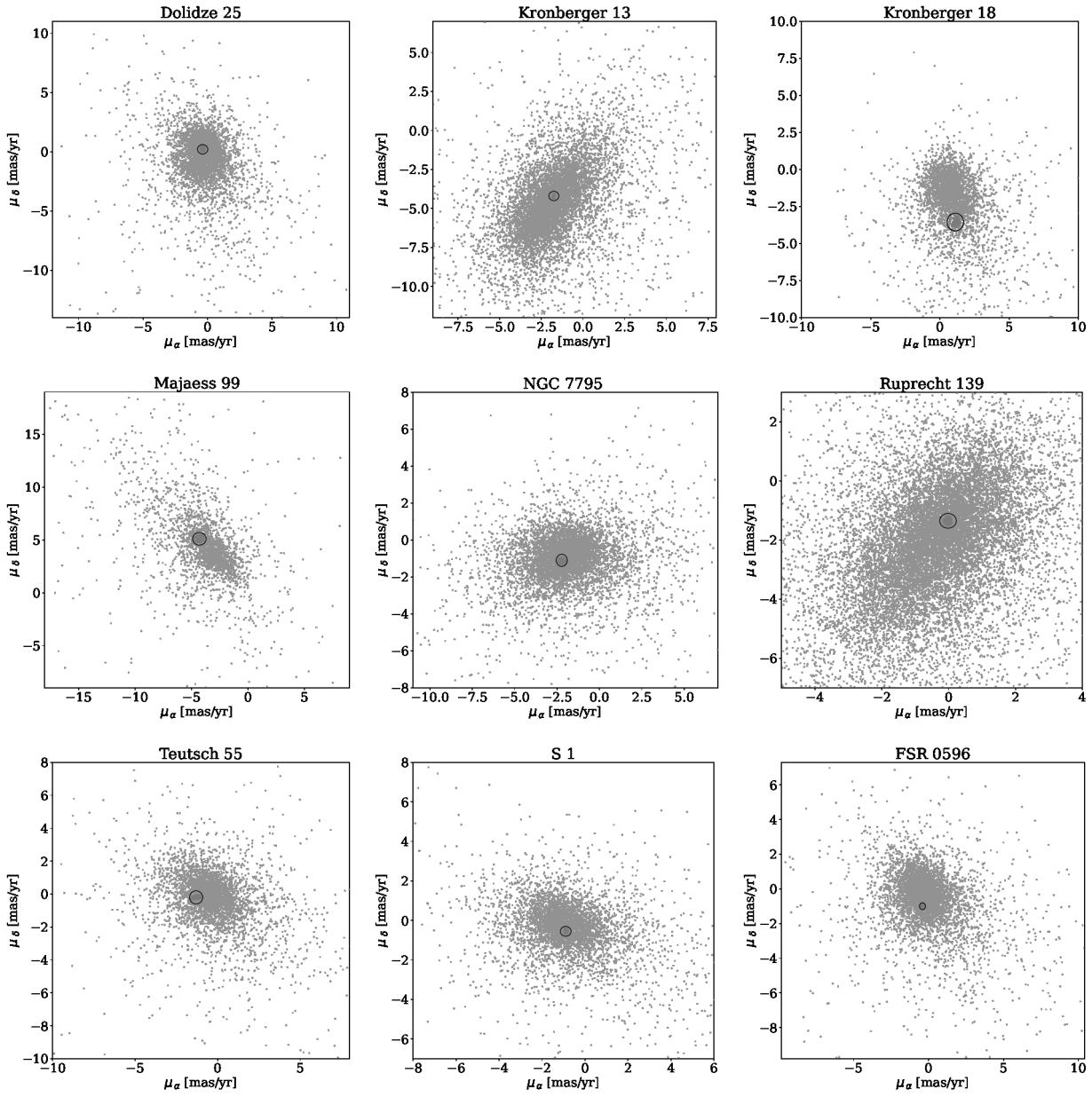

Fig. 2. The vector point diagrams (VPDs) of the studied clusters. The densest areas were placed in sub-circles with radii of 0.2 degrees.

stead of 3σ, some of the stars will be outside of the cluster's region and so they will not be considered member stars of the cluster. The parallax uncertainties are $0.02 - 0.03$ mas for $G < 15$, 0.07 mas at $G = 17$, 0.5 mas at $G = 20$, and 1.3 mas at G= 21 mag. We used only sources with parallaxes > 0. In their discussion of the conventional method of inverting parallaxes to determine distance, Luri et al. (2018) explain that the method is only accurate when there are no measurement uncertainties and when the distance is > 100 pc. It is not applicable for negative parallaxes arising from the survey's measurement process. The left hand side of Figure 4 shows the studied clusters' parallax range. Member stars are represented by blue dots, and background field stars are represented by yellow dots. The middle and right hand sides of Figure 4 show the stars' parallaxes in relation to their magnitudes and counts. Also, one of the parameters that must be taken into consideration is the value of the renor-

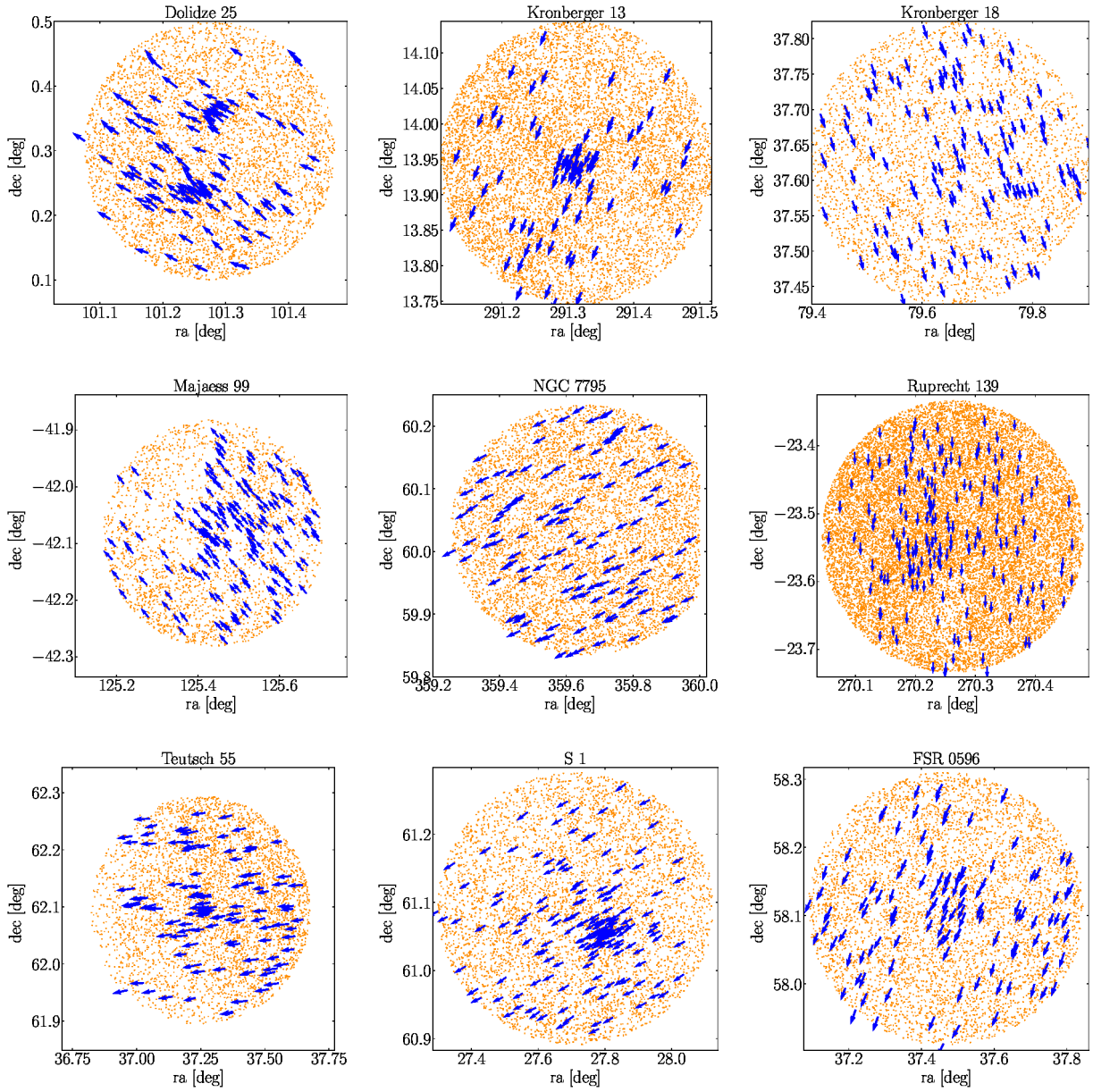

Fig. 3. Co-moving stars of the studied clusters. The blue arrows indicate the member stars as they move together in the same direction and speed, while the yellow dots show the background field stars. The color figure can be viewed online.

malized unit weight error, RUWE, which indicates that the single-star model provides a good fit to the astrometric observations, when it is ≤ 1.4 (Tadross and Elhosseiny 2022). As a result, these member stars form the usual shape for the color-magnitude diagram, CMD of the cluster, (Hendy and Tadross 2021). When the radius of the cluster is calculated (see § 3), all the stars that fall within this radius are regarded as member stars, and the stars outside this radius are regarded as background field stars.

3. OPEN CLUSTER SELECTION

Based on the Dias catalog (Dias et al. 2014), which has 2167 open clusters, we selected the current 9 open clusters that are close to the galactic plane and have members' proper motions separated from

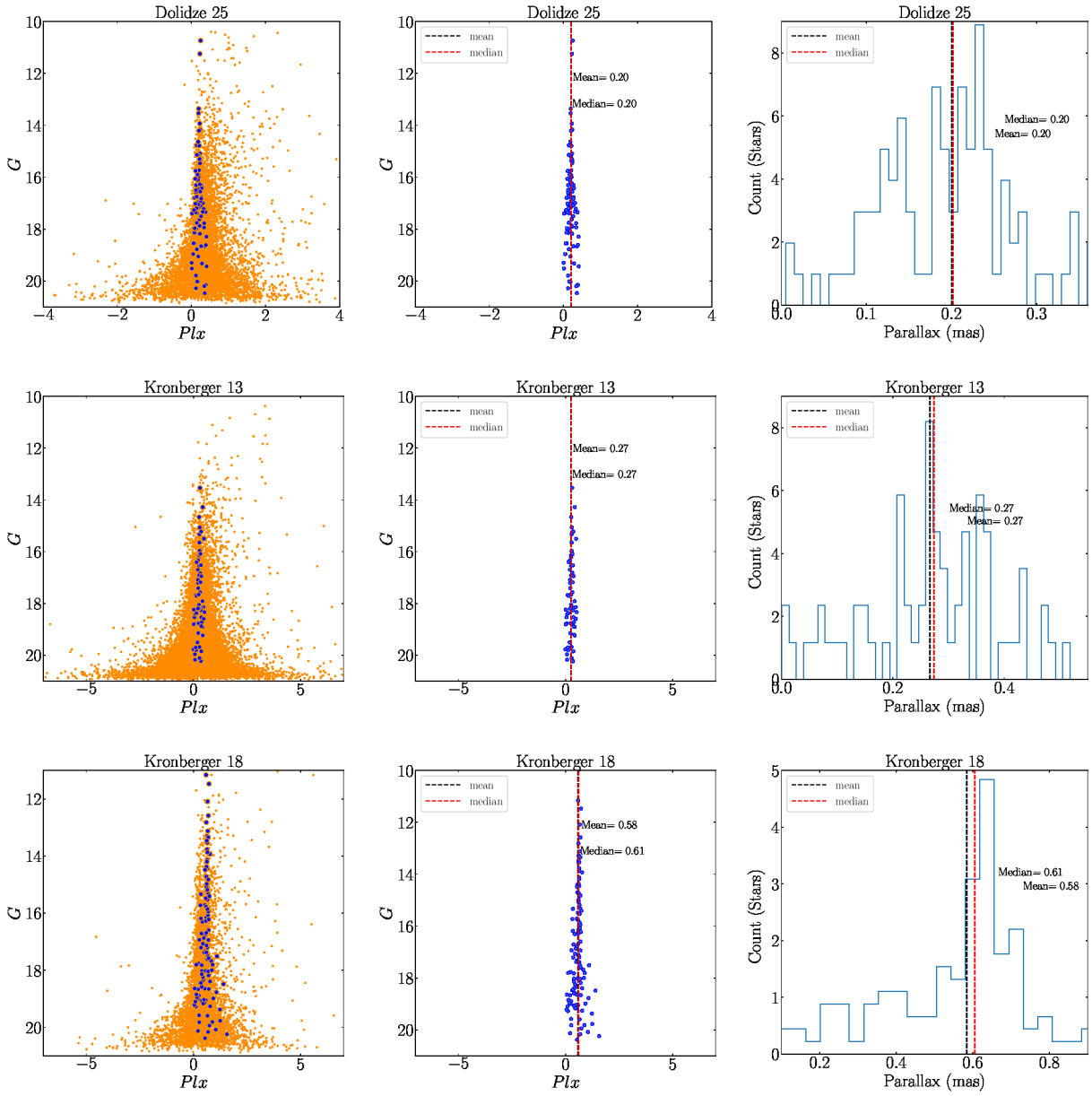

Fig. 4. The left-hand panels show the parallax range of studied clusters. The blue dots represent the member stars, while the yellow dots represent the background field stars. The middle and right hand panels show the parallax versus the magnitudes and the count numbers. The color figure can be viewed online.

the field stars. The quality of Gaia DR3 astrometry provides high accuracy proper motions in right ascension and declination (μ_α, μ_δ). Some OCs in Gaia, through, (Cantat-Gaudin et al. 2019) as well as OCs with unclear overdensities in VPDs, were excluded from our study. Kronberger13 and Ruprecht 139 are located in the first Galactic quadrant, and the rest of the clusters are located in the second Galactic quadrant.

The investigated nine open clusters, Dolidze 25 (Number=555 stars, Distance=6800 pc, E(B−V)=0.80 mag, log age=6.80 yr, Radius=10.50 arcmin). Kronberger 13 (Number=26 stars, Distance=1380 pc, E(B−V)= 1.13 mag, log age= 8.60 yr, Radius= 2.53 arcmin). Kronberger 18 (Number=40 stars, Distance= 3250 pc, E(B−V)=1.29 mag, log age= 8.00 yr, Radius=2.00 arcmin). Majaess 99 (Number=85 stars,

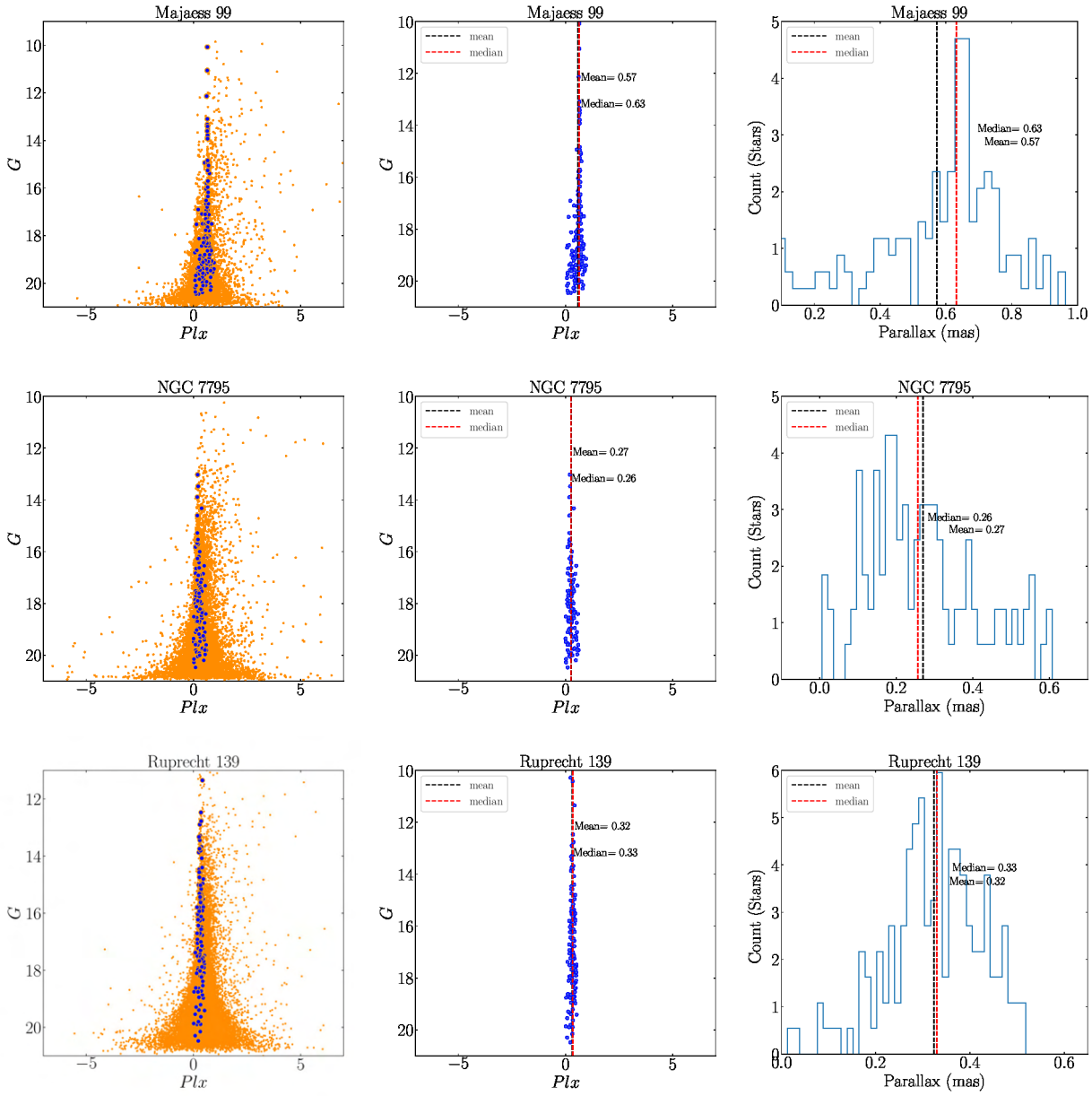

Fig. 4. Continued

Radius=5.50 arcmin). NGC 7795 (Number=806 stars, Distance=2105 pc, E(B−V)= 1.00 mag, log age=8.65 yr, Radius=11.00 arcmin). Ruprecht 139 (Number=1416 stars, Distance=550 pc, E(B−V)=0.15 mag, log age= 9.05 yr, Radius=11.58 arcmin). S1 (Number=101, Distance=2200 pc, E(B−V)=0.77 mag, log age= 7.40 yr, Radius=4.00 arcmin). Teutsch 55 (Number=80 stars, Distance=6020 pc, E(B−V)= 0.82 mag, log age=6.70 yr, Radius= 4.50 arcmin). FSR 0596 (Number=29 stars, Distance=1417 pc, E(B−V)=0.52 mag, log age=9.15 yr, Radius=2 arcmin). These OCs have been reported by Sampedro et al. (2017). A cluster may be difficult to find depending on a variety of parameters, including the density of the background, interstellar extinction, the population density, the age, and the proper motions of the field stars (Cantat-Gaudin et al. 2018).

4. SPATIAL STRUCTURE: CLUSTERS' SIZES, CENTERS, AND RICHNESS

Knowing cluster size is a substantial issue to investigate the cluster's dynamic evolution. It is hard

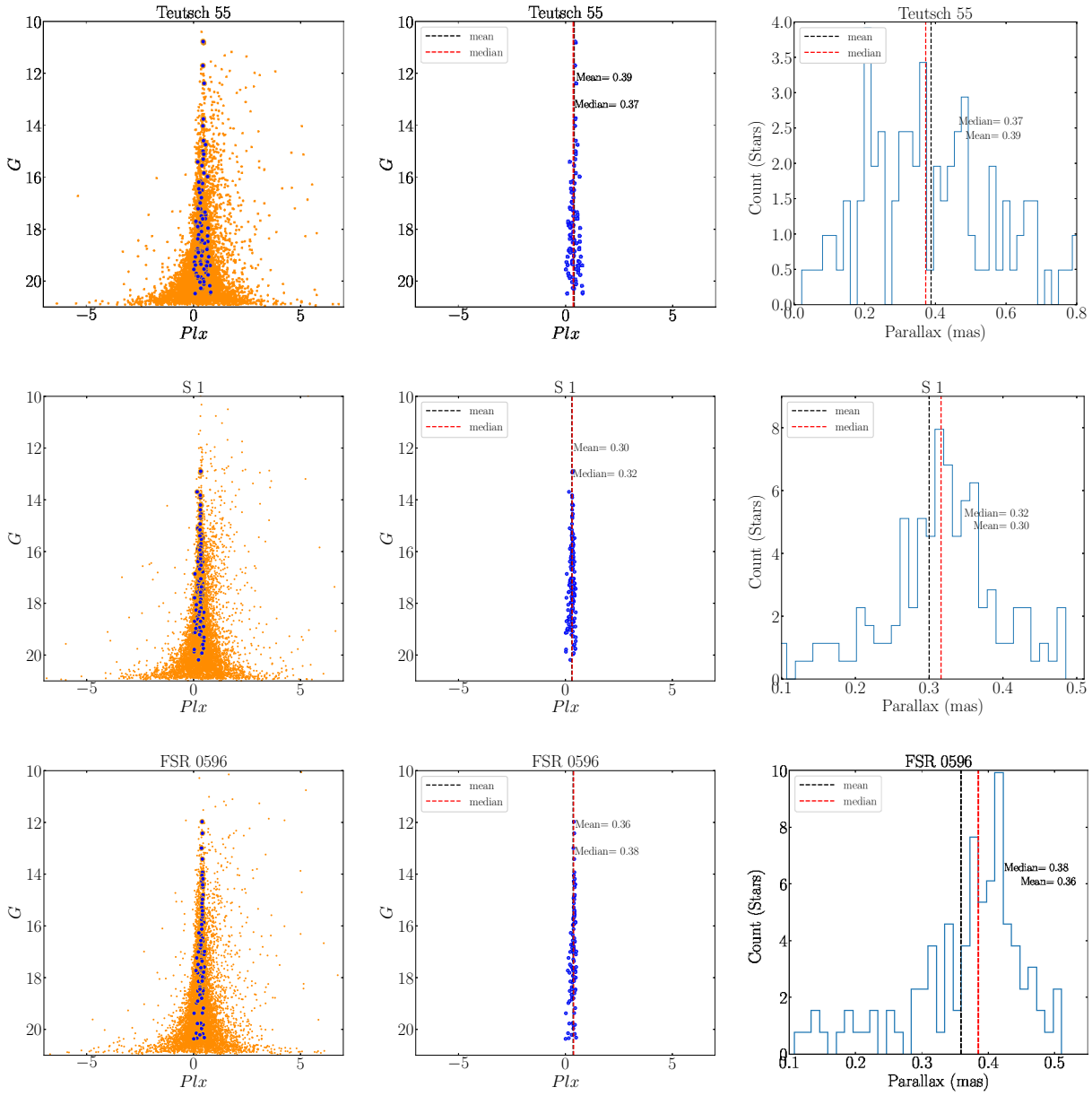

Fig. 4. Continued

to determine the precise cluster center and radial extent. Cluster radius estimation is one of the most significant basic parameters (Bisht et al. 2020). The cluster center is taken at the most over-condensation area of the cluster region taken from Dias' catalog. Subsequently, using Gaia DR3 data, we divided the area of the cluster into equal-sized bins in RA and Dec and counted the stars in each bin. The mean and median values have been applied to both RA and Dec. We estimated the radial stellar density profile (RDP) by estimating the stellar density in concentric circular rings centered at the cluster center. The number of stars in each annular region is counted (Joshi et al. 2012). The number density in the i zone is then $\rho_i = N_i/A_i$, where N_i and A_i are the star number and the area of the i zone, respectively. The error bars are derived supposing that the number of stars in an area follows the Poisson error. The limiting radius R_{lim} could be estimated to cover the entire cluster region and reached a sufficient stability, where the member stars merge with the field ones (Tadross and Hendy 2022). Therefore, R_{lim}

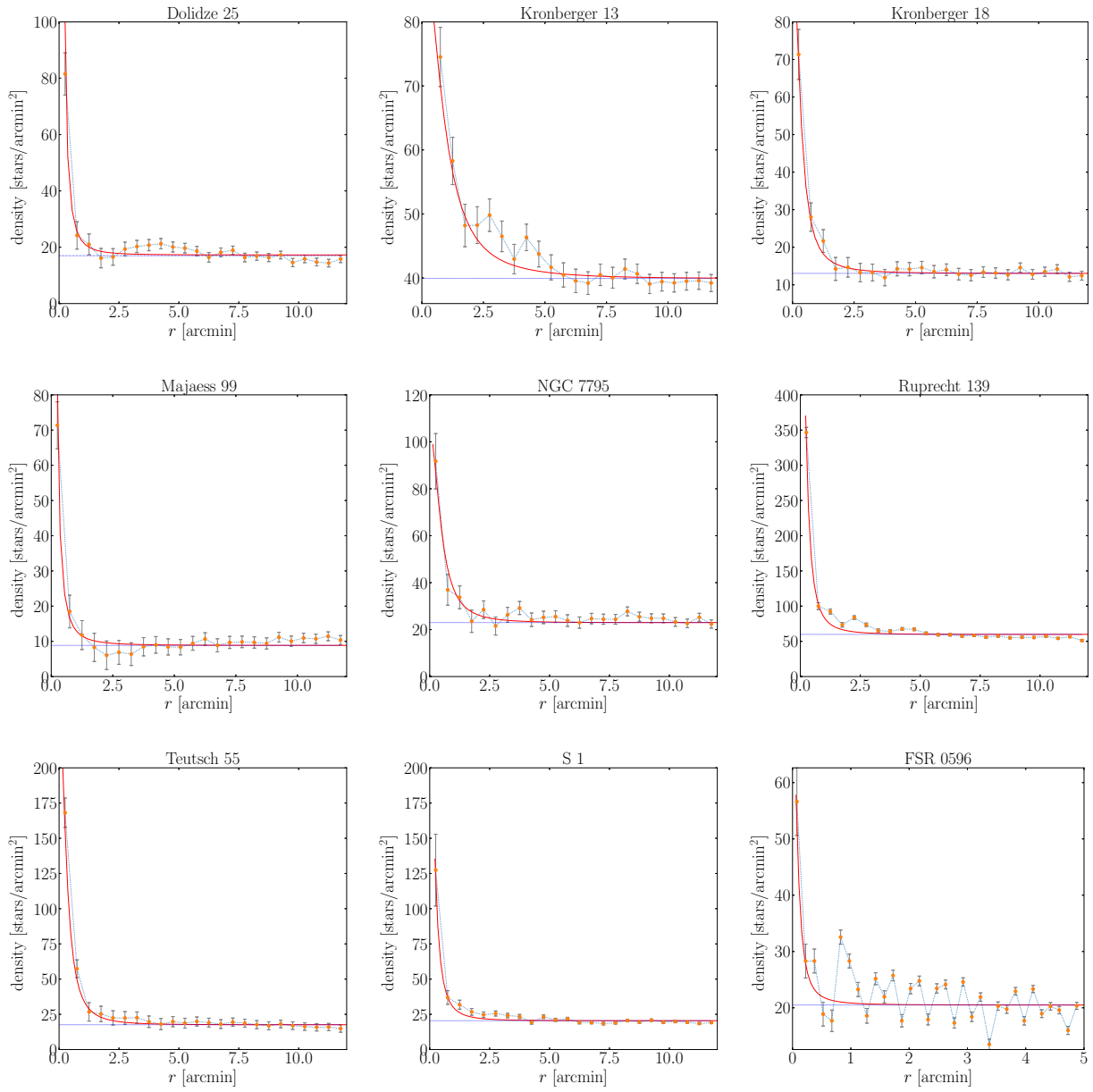

Fig. 5. The RDP curves of the studied clusters. Errors are determined by the relation $(1/\sqrt{N})$, where N is the number of cluster member stars in each radial bin. The King profile (1966) is represented by the red line, while the background density is represented by the blue line. The color figure can be viewed online.

was calculated according to the following formula of Bukowiecki et al. (2011); we can get the boundary radius by applying the equation as follows:

$$R_{lim} = R_c \sqrt{\frac{f_o}{3\sigma_{bg}} - 1}, \quad (1)$$

where σ_{bg} is the uncertainty of the f_b value. So, the estimated radius of such cluster is just a minimum radial range of the cluster (Maurya and Joshi 2020).

The spatial structure and radial density of the OCs were derived by fitting the RDP given by King (1966) as follows:

$$f(R) = f_b + \frac{f_o}{1 + (\frac{R}{R_c})^2}, \quad (2)$$

where f_b, f_o, and R_c are the background field density, central star density and the core radius of the cluster, which is defined as the radial distance from

TABLE 1

THE STRUCTURE PARAMETERS' VALUES OF THE STUDIED CLUSTERS

Cluster	f_o	f_b	R_{lim}	R_c	R_t	C
...	star/arcmin^2	star/arcmin^2	arcmin	arcmin	arcmin	...
Dolidze 25	81.75	4.27	5.40	0.12	7.12	1.65
Kronberger 13	85.24	39.93	5.25	0.89	6.27	0.77
Kronberger 18	89.74	13.04	4.80	0.34	7.60	1.15
Majaess 99	341.84	8.85	4.20	0.12	7.71	1.54
NGC 7795	3.83	1.81	4.28	0.50	6.33	0.32
Ruprecht 139	640.91	59.90	3.70	0.21	11.52	1.24
Teutsch 55	242.59	17.62	4.30	0.32	7.84	1.13
S 1	242.89	20.49	4.30	0.22	8.70	1.29
FSR 0596	55.00	20.49	3.53	0.09	6.36	1.59

TABLE 2

THE PASSBANDS FOR THE GAIA FILTER

Filter	G	G_{BP}	G_{RP}
A_λ/A_V	0.83627	1.08337	0.63439

the center where the stellar density $f(R)$ becomes half of its central value f_o. The estimated values of the structural parameters are reported in Table 1 for all the clusters. The stellar density distributions for the studied clusters are shown in Figure 5 where the solid red curves are the King profiles. Furthermore, the tidal radius of the cluster R_t is the distance from the core of the cluster, where the effect of gravity for the Galaxy is equal to that of the cluster. With the mass calculation of these clusters, the tidal radius can be estimated by using Jeffries et al. (2001) equation as follows:

$$R_t = 1.46 \times (M_c)^{\frac{1}{3}}, \quad (3)$$

where R_t and M_c are the tidal radius (in parsecs) and the total mass of the cluster (in solar masses). The concentration parameter C indicates how the member stars are prominent compared with the field stars; based on Peterson and King (1975), we can obtain the concentration parameter as follows:

$$C = \log\left(\frac{R_{lim}}{R_c}\right). \quad (4)$$

5. COLOR-MAGNITUDE DIAGRAM, AGE AND DISTANCE

The distances and ages of the Galactic OCs are important parameters when using them as tracers to investigate the structure and chemical evolution of the Galaxy. The analysis of the color-magnitude diagram (CMD) is a commonly used method for analyzing the observable main sequence of a cluster. Due to their sharing the same origin, the cluster members move through space in the same direction and at the same speed. It is necessary to identify which star evolutionary isochrones (from the COLIBRI tracks of Marigo et al. 2017) match well the cluster's main-sequence curve (CMD 3.6 input form)[6]. To lessen the impact of field stars contamination only the cluster members are used. By fitting the theoretical isochrones of solar metallicity $Z = 0.0152$ provided by Marigo et al. (2017) on the CMD of the clusters, the ages and distances of the clusters have been determined. The passbands of the Gaia filters are obtained from Riello et al. (2021), as listed in Table 2. To achieve the best fit while changing the isochrone of a given age for different distance-modulus, the reddening $E(G_{BP}-G_{RP})$ values established are employed as reported in Table 3. The presence of interstellar dust lying along the line of sight of the cluster reddens the observed magnitudes and colors due to the scattering of background star light by dust particles. The redding values are taken from the isochrones fitting to the CMD of the studied clusters. The red lines in Figure 6 show the best fitting isochrones to the CMDs of the studied clusters.

To calculate the true distance to the cluster, the apparent distance modulus must be corrected for the reddening parameter, which has a significant impact on the total absorption value, $(m-M)_o = (m-M) - A_G$, where $A_G = 1.86E(G_{BP}-G_{RP})$. By converting the current color excess to $E(B-V)$ and correcting the magnitudes for interstellar reddening, these ratios have been employed, with $A_V = R_V E(B-V)$, where $R_V = 3.1$.

[6] http://stev.oapd.inaf.it/cgi-bin/cmd

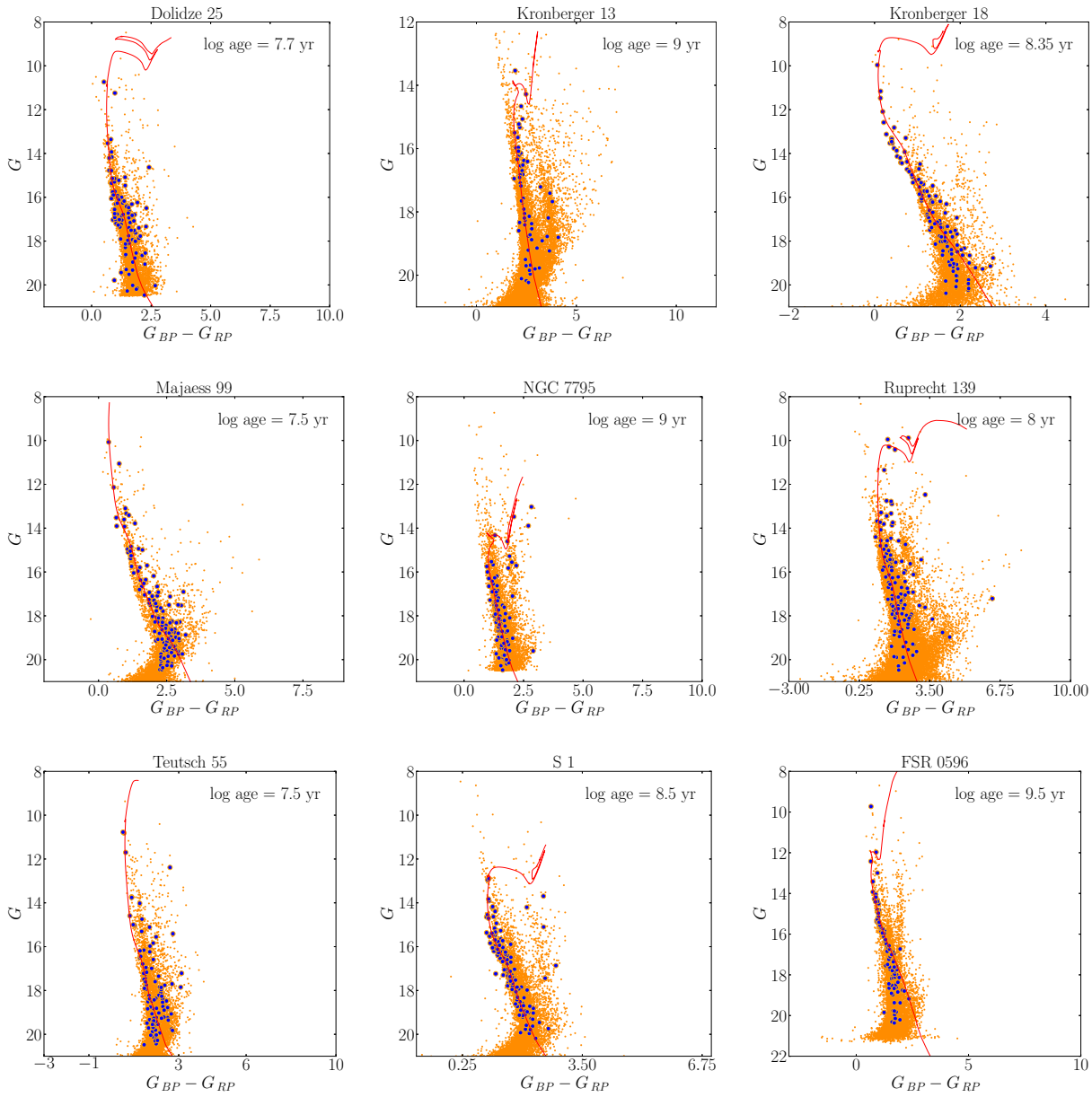

Fig. 6. The color-magnitude diagrams of the studied clusters. Probable cluster members are represented by blue dots which are obtained from the VPDs. The color figure can be viewed online.

As reported in Table 3, the estimated Cartesian Galactocentric coordinates ($X_\odot$, $Y_\odot$, $Z_\odot$) and distances from the Galactic center (R_{GC}) are provided. The calculation of cluster's geometric distances has been taken from Tadross (2011). The distance between the Sun and the Galactic core is $R_o = 8.20$ kpc (Bland-Hawthorn et al. 2019). The distance from the Sun, $R_\odot$, the axes of the projected rectangular distances on the Galactic plane, $X_\odot$ and $Y_\odot$, and the distance from the Galactic plane, $Z_\odot$, are known as the Galactic geometric distances. Such distances are significant for studying the Galaxy's structure or the traces left by the Milky Way arms.

6. LUMINOSITY FUNCTION

The total number of a cluster stars across all magnitude bins is known as the luminosity function (LF). Figure 7 provides the predicted LF for

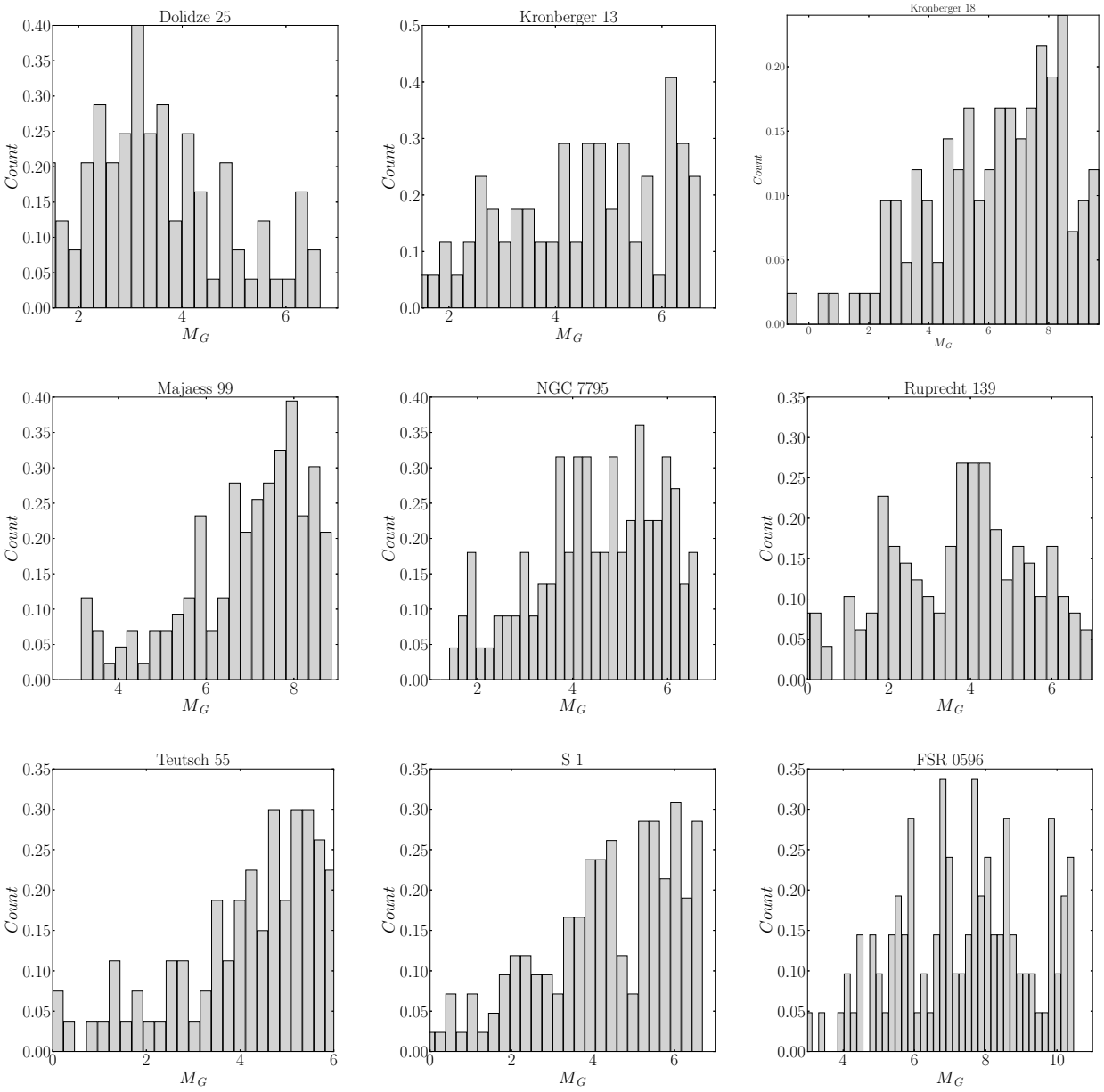

Fig. 7. The luminosity functions of the main-sequence stars of the studied clusters.

the studied clusters. The LF shows how the cluster members absolute magnitudes are distributed. The apparent G magnitudes of the cluster members were converted into absolute magnitudes using the distance moduli determined through isochrone fitting, $M_g = G - (m - M)$. By using the data from the isochrones of Marigo et al.(2017) at the cluster's age, it is possible to determine the luminosities and masses of the cluster members. For the most effective potential estimates of the LF and mass function (MF) which will be mentioned in the next section, the magnitude bin intervals are chosen to be suitable for stars in each bin. Table 3 shows the LF and MF derived for the studied clusters.

7. MASS FUNCTION

Understanding the process of star formation and the subsequent chemical and dynamical evolution of the star clusters depends heavily on the initial mass function (IMF) investigations Kroupa (2002). The

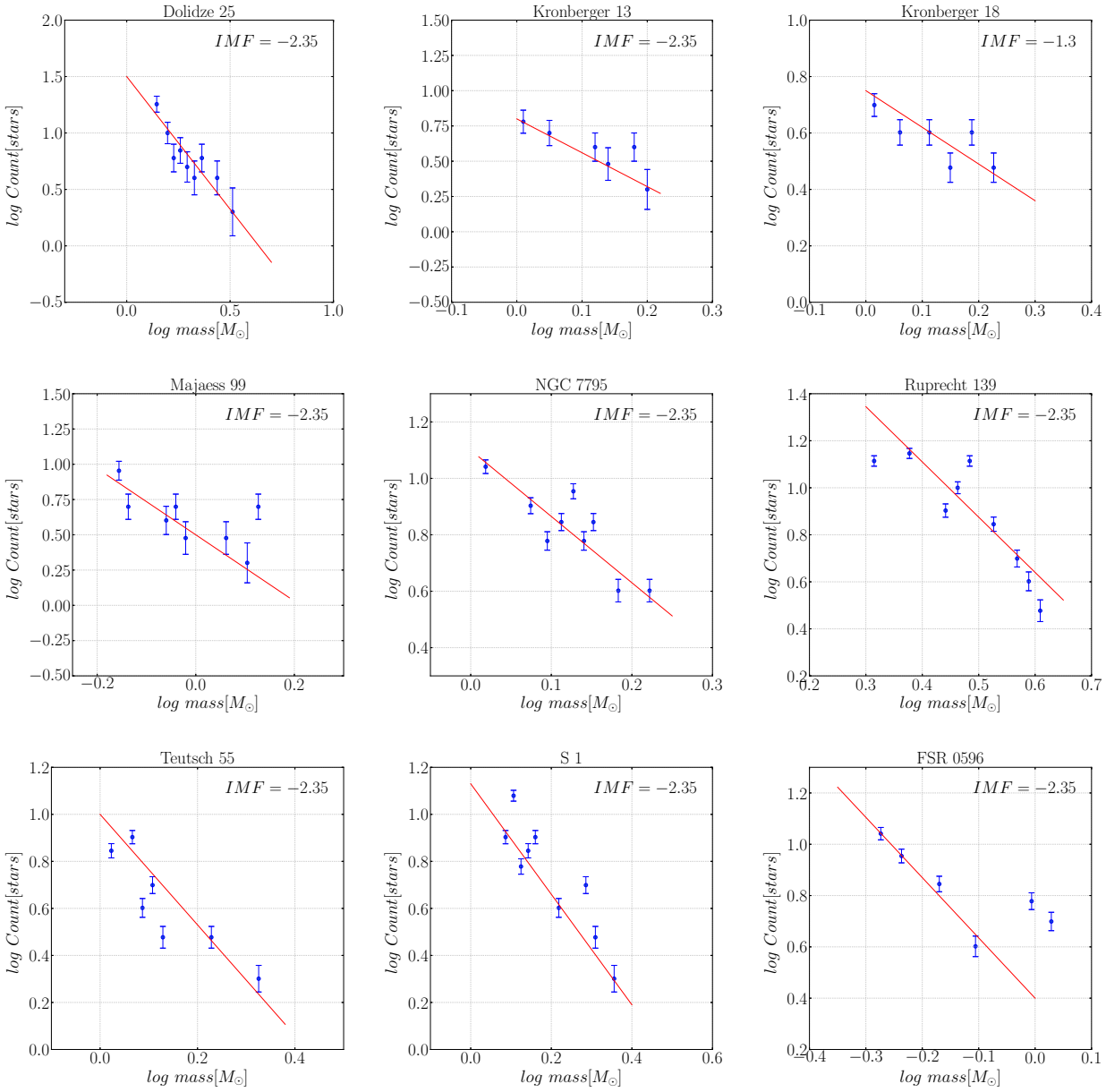

Fig. 8. The initial mass function slopes of the studied clusters. The error bars determined from the relation $1/\sqrt{N}$, where N is the number of the cluster members in each mass bin. The color figure can be viewed online.

primary link between the bright, massive members and the less massive, fainter members is provided by the IMF. It is essential for understanding the early dynamic evolution of star clusters and acts as historical evidence of the star formation process. Due to the dynamic evolution of the star system, a direct determination of IMF for the cluster is not feasible. According to Salpeter (1955) power law, which states that the number of stars in each mass range declines as the mass increases, the IMF was calculated for the bright massive stars $> 1M_{\odot}$. Comparing the color and magnitude of each star to the theoretical solar metallicity isochrones (Marigo et al. 2017) at the estimated age, we were able to determine the mass of each star photometrically. On the chosen isochrones, the mass of each cluster member was calculated from its closest neighbour. As a result, we calculated the current MF, which is the number of stars per mass

TABLE 3

THE PHYSICAL PARAMETERS'VALUES OF THE STUDIED CLUSTERS

Cluster	$ra(2000)$	$dec(2000)$	$l(2000)$	$b(2000)$	$E(BP-RP)$	$(m-M)$	A_G	d	Plx
...	$degree$	$degree$	$degree$	$degree$	mag	mag	mag	PC	mas
Dolidze 25	101.27	0.30	211.94	-1.27	0.90	13.80	1.67	2666	0.27
Kronberger 13	291.31	13.94	49.17	-0.98	1.60	13.5	2.98	1270	0.34
Kronberger 18	79.65	37.62	169.64	0.03	0.20	10.70	0.37	1164	0.58
Majaess 99	125.44	-42.08	259.60	-2.98	0.69	11.60	1.28	1158	0.63
NGC 7795	359.65	60.035	116.37	-2.16	0.75	13.86	1.39	3104	0.27
Ruprecht 139	270.26	-23.53	6.41	-0.23	1.30	13.50	2.42	1644	0.39
Teutsch 55	37.25	62.09	134.08	1.35	0.92	13.70	1.71	2500	0.43
S 1	27.71	61.09	130.05	-0.96	1.00	13.80	1.86	2443	0.41
FSR 0596	37.47	58.11	135.65	-2.31	0.03	10.00	0.05	977	0.41

TABLE 3. CONTINUED

Cluster	T_R	$logage$	τ	N	M_v	M_C	IMF	μ_α	μ_δ
...	Myr	yr	...	$Stars$	mag	$M_\odot$	...	mas/yr	mas/yr
Dolidze 25	12.55	7.70	3.99	81	-2.01	116.07	-2.35	-0.40	0.33
Kronberger 13	4.59	9.00	217.86	77	-6.06	79.33	-2.40	-1.76	-4.21
Kronberger 18	3.57	8.35	62.71	120	-4.08	141.24	-1.30	1.11	-3.55
Majaess 99	3.17	7.50	9.97	155	-3.71	147.34	-2.35	-4.31	5.13
NGC 7795	12.81	9.00	78.06	108	-3.83	145.76	-2.35	-10.81	-2.87
Ruprecht 139	2.86	8.00	34.96	175	-8.16	491.01	-2.35	0.02	-1.37
Teutsch 55	6.16	7.50	5.13	110	-5.71	155	-2.35	-1.22	0.18
S 1	8.58	8.50	36.83	160	-5.33	212.46	-2.35	-0.74	-0.83
FSR 0596	2.06	9.50	1534.95	116	-1.76	82.79	-2.35	-0.41	-0.98

TABLE 3. CONTINUED

Cluster	$X_\odot$	$Y_\odot$	$Z_\odot$	R_{GC}
...	pc	pc	pc	kpc
Dolidze 25	-2261.82	-1410.05	-59.09	10.56
Kronberger 13	830.21	960.81	-21.71	19.19
Kronberger 18	-1145.02	209.32	0.61	21.15
Majaess 99	-208.76	-1137.43	-60.20	8.48
NGC 7795	-1377.71	2779.03	-116.99	9.97
Ruprecht 139	1633.71	183.54	-6.60	18.37
Teutsch 55	-1738.67	1795.42	58.90	10.10
S 1	-1571.74	1869.81	-4.93	9.95
FSR 0596	-698.07	682.41	-39.38	20.71

bin, and is frequently described by the power law $\frac{dN}{dM} \propto m^{-\alpha}$, where α is the slope of MF. It can be given as

$$\log \frac{dN}{dM} = -\alpha \log M + Constant, \qquad (5)$$

where $\log(dN)$ is the logarithmic number of stars per unit logarithmic mass interval (dM). Salpeter (1955) determined the slope of the mass function α as -2.35 among the solar neighborhood stars, which is typically regarded as a classical value of the MF slope, for the mass range $0.4 < M/M_\odot \leq 10$. We determined the mean mass in each magnitude bin of the G band. We provide the mass range, mean mass, and cluster members in different brightness range for the clusters. The two-stage power law in

some of the MF slopes of OCs may be due to the dynamics of clusters and/or to initial conditions in star formation events (Bonatto & Bica 2005). The resulting mass function obtained for the clusters is shown in Figure 8.

8. THE DYNAMIC RELAXATION TIME

The dynamic relaxation time T_R is the time during which the velocity distribution of stars in a cluster approaches its equilibrium distribution. We estimated the dynamic relaxation time to determine if the mass segregation process in the clusters is caused by dynamical development or by the star formation process itself. According to Spitzer and Hart (1971), the relaxation time, T_R, is mathematically defined as

$$T_R = \frac{8.9 \times 10^5 \times \sqrt{N} \times R_h^{1.5}}{\sqrt{\overline{m}} \times \log(0.4 \times N)}, \quad (6)$$

where N is the total number of stars in the cluster. R_h is the star cluster's half-mass radius, and $\overline{m}$ is the average stellar mass in the cluster. To calculate R_h, we first added up the masses of each cluster member individually and calculated both the mean stellar mass and the total mass of each cluster. After determining the radius where 50% of the cluster's total mass is included, we can get R_h values, and then T_R can be obtained. We can define the dynamical evolution parameter from the following relation based on the cluster age and its relaxation time

$$\tau = \frac{age}{T_R}. \quad (7)$$

9. CONCLUSIONS

The main astrophysical parameters of the nine open stellar clusters Dolidze 25, Kronberger 13, Kronberger 18, Majaess 99, NGC 7795, Ruprecht 139, Teutsch 55, S1, and FSR 0596 were estimated in this paper for the first time using the Gaia DR3 database. Comparing the astrometric parameters obtained here for 5 OCs (Kronberger 18, Majaess 99, NGC 7795, Ruprecht 139, and Teutsch 55) with those provided by Dias et al. (2018). Kronberger 18 (radius = 3 arcmin, μ_α = 2.01 mas/yr, μ_δ = −3.89 mas/yr, number = 49 stars). Majaess 99 (radius = 6 arcmin, μ_α = −6.21 mas/yr, μ_δ = 5.56 mas/yr, number = 69 stars). NGC 7795 (radius = 11.5 arcmin, μ_α = −1.57 mas/yr, μ_δ = −0.95 mas/yr, number = 879 stars). Ruprecht 139 (radius = 7 arcmin, μ_α = −0.21 mas/yr, μ_δ = −2.31 mas/yr, number = 658 stars). Teutsch 55 (radius = 5 arcmin, μ_α = −1.11 mas/yr, μ_δ = −0.29 mas/yr, number = 87 stars) it is clear that they are well consistent with our results. Dolidze 25, S1, FSR 0596, and Kronberger 13 are not found in that catalog. Majaess 99 was reported only by Monteiro and Dias (2019); their results are in good agreement with ours as well. Majaess 99 (log age = 6.66 ± 0.01 yr, distance = 1.32 ± 0.08 kpc, $E(B\text{-}V)$ = 0.02 ± 0.02 mag, number = 46 stars, $\mu_\alpha = -4.37 \pm 0.002$ mas/yr, $\mu_\delta = 5.19 \pm 0.01$ mas/yr, parallax = 0.66 ± 0.03 mas). All the parameters of our studied clusters are summarized and listed in Table 3.

This work has made use of data from the European Space Agency (ESA) mission Gaia processed by the Gaia Data Processing and Analysis Consortium (DPAC), https://www.cosmos.esa.int/web/gaia/dpac/consortium. Funding for the DPAC has been provided by national institutions, in particular, the institutions participating in the Gaia Multilateral Agreement (MLA).

REFERENCES

Badawy, W. A., Tadross, A. L., Hendy, Y. H. M., et al. 2022, JAsGe, 11, 142

Bate, M. R., Bonnell, I. A., & Bromm, V. 2003, MNRAS, 339, 577, https://doi.org/10.1046/j.1365-8711.2003.06210.x

Bisht, D., Elsanhoury, W. H., Zhu, Q., et al. 2020, AJ, 160, 119, https://doi.org/10.3847/1538-3881/ab9ffd

Bisht, D., Zhu, Q., Yadav, R. K. S., Durgapal, A., & Rangwal, G. 2020, MNRAS, 494, 607, https://doi.org/10.1093/mnras/staa656

Bland-Hawthorn, J., Sharma, S., Tepper-García, T., et al. 2019, MNRAS, 486, 1167, https://doi.org/10.1093/mnras/stz217

Bonatto, C. & Bica, E. 2005, A&A, 437, 483, https://doi.org/10.1051/0004-6361:20042516

Bonatto, C., Kerber, L. O., Bica, E., & Santiago, B. X. 2006, A&A, 446, 121, https://doi.org/10.1051/0004-6361:20053573

Bossini, D., Vallenari, A., Bragaglia, A., et al. 2019, A&A, 623, 108, https://doi.org/10.1051/0004-6361/201834693

Bragaglia, A. 2017, IAUS 330, Astrometry and Astrophysica in the Gaia Sky, 119, https://doi.org/10.1017/s1743921317005294

Bressan, A., Marigo, P., Girardi, L., et al. 2012, MNRAS, 427, 127, https://doi.org/10.1111/j.1365-2966.2012.21948.x

Bukowiecki, Ł., Maciejewski, G., Konorski, P., & Strobel, A. 2011, AcA, 61, 231, https://doi.org/10.48550/arXiv.1107.5119

Cantat-Gaudin, T., Jordi, C., Vallenari, A., et al. 2018, A&A, 618, 93, https://doi.org/10.1051/0004-6361/201833476

Cantat-Gaudin, T., Anders, F., Castro-Ginard, A., et al. 2020, VizieR Online Data Catalog: Portrait Galactic disc (Cantat-Gaudin+, 2020)

Dias, W. S., Monteiro, H., Caetano, T. C., et al. 2014, A&A, 564, 79, https://doi.org/10.1051/0004-6361/201323226

Dias, W. S., Alessi, B. S., Moitinho, A., & Lepine, J. R. D. 2014, VizieR Data Catalog: Optically visible open clusters and Candidates (Dias+2002-2015)

Dias, W. S., Monteiro, H., & Assafin, M. 2018, MNRAS, 478, 5184, https://doi.org/10.1093/mnras/sty1456

Gaia Collaboration, Vallenari, A., Brown, A. G. A. et al. 2022, arXiv, https://doi.org/10.48550/arXiv.2208.00211

Harris, W. E. & Pudritz, R. E. 1994, ApJ, 429, 177, https://doi.org/10.1086/174310

Hendy, Y. & Tadross, A. 2021, AN, 342, 613, https://doi.org/10.1002/asna.202143848

Hills, S., von Hippel, T., Courteau, S., & Geller, A. M. 2015, AJ, 149, 94, https://doi.org/10.1088/0004-6256/149/3/94

Jeffries, R. D., Thurston, M. R., & Hambly, N. C. 2001, A&A, 375, 863, https://doi.org/10.1051/0004-6361:20010918

Joshi, Y. C., Joshi, S., Kumar, B., Mondal, S., & Balona, L. A. 2012, MNRAS, 419, 2379, https://doi.org/10.1111/j.1365-2966.2011.19890.x

King, I. R. 1966, AJ, 71, 64, https://doi.org/10.1086/109857

Kroupa, P. 2002, Sci, 295, 82, https://doi.org/10.1126/science.1067524

Luri, X., Brown, A. G. A., Sarro, L. M., et al. 2018, A&A, 616, 9, https://doi.org/10.1051/0004-6361/201832964

Marigo, P., Girardi, L., Bressan, A., et al. ApJ, 835, 77, https://doi.org/10.3847/1538-4357/835/1/77

Maurya, J. & Joshi, Y. C. 2020, MNRAS, 494, 4713, https://doi.org/10.1093/mnras/staa893

Monteiro, H. & Dias, W. S. 2019, MNRAS, 487, 2385, https://doi.org/10.1093/mnras/stz1455

Peterson, C. J. & King, I. R. 1975, AJ, 80, 427, https://doi.org/10.1086/111759

Riello, M., De Angeli, F., Evans, D. W., et al. 2021, A&A, 649, 3, https://doi.org/10.1051/0004-6361/202039587

Salpeter, E. E. 1955, ApJ, 121, 161, https://doi.org/10.1086/145971

Sampedro, L., Dias, W. S., Alfaro, E. J., Monteiro, H., & Molino, A. 2017, MNRAS, 470, 3937, https://doi.org/10.1093/mnras/stx1485

Spitzer, L. Jr. & Hart, M. H. 1971, ApJ, 164, 399, https://doi.org/10.1086/150855

Straižys, V., Boyle, R. P., Milašius, K., et al. 2019, A&A, 623, 22, https://doi.org/10.1051/0004-6361/201833987

Tadross, A. L. 2011, JKAS, 44, 1, https://doi.org/10.5303/JKAS.2011.44.1.1

_____. 2018, RAA, 18, 158, https://doi.org/10.1088/1674-4527/18/12/158

_____. 2021, JApA, 42, 6, https://doi.org/10.1007/s12036-020-09648-5

_____. 2022, AdSpR, 69, 467, https://doi.org/10.1016/j.asr.2021.09.014

Tadross, A. L. & Elhosseiny, E. G. 2022, RMxAA, 58, 387, https://doi.org/10.22201/ia.01851101p.2022.58.02.17

Yadav, R. K. S., Sariya, D. P., & Sagar, R. 2013, MNRAS, 430, 3350, https://doi.org/10.1093/mnras/stt136

W. A. Badawy, Y. H. M. Hendy, and A. L. Tadross: National Research Institute of Astronomy and Geophysics, Cairo, Egypt.

M. N. Ismail and A. Mouner: Faculty of Science, Al-Azhar University, Cairo, Egypt.